www.elsevier.com/locate/yjtbi

A multiscale model of placental oxygen exchange: The effect of villous tree structure on exchange efficiency

Mabelle Lin, Benjamin Mauroy, Joanna L. James, Merryn H. Tawhai, Alys R. Clark

PII: S0022-5193(16)30171-0
DOI: http://dx.doi.org/10.1016/j.jtbi.2016.06.037
Reference: YJTBI8725

To appear in: *Journal of Theoretical Biology*

Received date: 29 January 2016
Revised date: 29 June 2016
Accepted date: 30 June 2016

Cite this article as: Mabelle Lin, Benjamin Mauroy, Joanna L. James, Merryn H Tawhai and Alys R. Clark, A multiscale model of placental oxygen exchange: The effect of villous tree structure on exchange efficiency, *Journal of Theoretica Biology,* http://dx.doi.org/10.1016/j.jtbi.2016.06.037

A multiscale model of placental oxygen exchange: The effect of villous tree structure on exchange efficiency

Mabelle Lin[a], Benjamin Mauroy[b], Joanna L. James[c], Merryn H. Tawhai[a], Alys R. Clark[a,*]

[a] *Auckland Bioengineering Institute, The University of Auckland, Auckland, New Zealand*
[b] *Laboratoire J. A. Dieudonné - UMR CNRS 7351, Université de Nice-Sophia Antipolis, Nice, France*
[c] *Department of Obstetrics and Gynaecology, Faculty of Medical and Health Sciences, University of Auckland, New Zealand*

Abstract

The placenta is critical to fetal health during pregnancy as it supplies oxygen and nutrients to maintain life. It has a complex structure, and alterations to this structure across spatial scales are associated with several pregnancy complications, including intrauterine growth restriction (IUGR). The relationship between placental structure and its efficiency as an oxygen exchanger is not well understood in normal or pathological pregnancies. Here we present a computational framework that predicts oxygen transport in the placenta which accounts for blood and oxygen transport in the space around a placental functional unit (the villous tree). The model includes the well-defined branching structure of the largest villous tree branches, as well as a smoothed representation of the small terminal villi that comprise

*Corresponding author
Email addresses: mlin865@aucklanduni.ac.nz (Mabelle Lin), benjamin.mauroy@unice.fr (Benjamin Mauroy), j.james@auckland.ac.nz (Joanna L. James), m.tawhai@auckland.ac.nz (Merryn H. Tawhai), alys.clark@auckland.ac.nz (Alys R. Clark)

the placenta's gas exchange interfaces. The model demonstrates that oxygen exchange is sensitive to villous tree geometry, including the villous branch length and volume, which are seen to change in IUGR. This is because, to be an efficient exchanger, the architecture of the villous tree must provide a balance between maximising the surface area available for exchange, and the opposing condition of allowing sufficient maternal blood flow to penetrate into the space surrounding the tree. The model also predicts an optimum oxygen exchange when the branch angle is 24°, as villous branches and TBs are spread out sufficiently to channel maternal blood flow deep into the placental tissue for oxygen exchange without being shunted directly into the DVs. Without concurrent change in the branch length and angles, the model predicts that the number of branching generations has a small influence on oxygen exchange. The modelling framework is presented in 2D for simplicity but is extendible to 3D or to incorporate the high-resolution imaging data that is currently evolving to better quantify placental structure.

Highlights

- A new oxygen exchange model incorporating a villous tree structure is proposed.
- Key associations between oxygen exchange and villous tree structure are identified.
- Villous tree structure influences intervillous blood flow and oxygen uptake capacity.

Keywords:

Placenta, Placental structure, Intervillous blood flow, Gas exchange, Computational model

1. Introduction

The human placenta is crucial for the survival and health of a fetus. It is the only exchange interface that provides the fetus with nutrients and oxygen during pregnancy. Numerous pregnancy complications such as preeclampsia and intrauterine growth restriction (IUGR) have been associated with placental malfunction [1]. While morphological abnormalities have been identified in pathological placentas [2, 3, 4], it is not fully understood how these translate to abnormalities in placental function.

Figure 1a shows a schematic of placental structure. It contains numerous branching structures known as chorionic villous trees, each of which comprises a network of fetal blood vessels. The largest branches of the villous trees (termed stem and intermediate villi) contain one or more arteriole or venule, and these blood vessels branch along with the villous tree structure. In the smallest villi (terminal villi), dilated capillary convolutes reside close to the villus surface. This surface is covered by a single multinucleated cell layer called the syncytiotrophoblast. The proximity of blood vessels to the surface of the villous tree provides an exchange interface to extract oxygen and nutrients from maternal blood that flows through the intervillous space (IVS) surrounding the villous trees, while keeping the fetal circulation separate from the maternal circulation.

Morphological abnormalities associated with pathology include reduced volume and surface area of terminal villi [2, 4], decreased villus length [2, 4],

increased trophoblast epithelium thickness [2] and abnormally sparse capillary networks [3, 5]. However, the relationship between these villus abnormalities and the functionality of the placenta is not well defined. Most animal models of the placenta are difficult to extrapolate to human because the placenta displays a wide structural diversity between species [6]. For ethical reasons, it is also impossible to perform invasive experiments or collect measurements directly from the human fetus or placenta during the course of pregnancy. Therefore, although the placenta can be imaged *in vivo* using ultrasound [7] and magnetic resonance imaging [8], the resolution of these techniques is currently not sufficient to relate the *in vivo* orientation of villous trees to incoming flow from the maternal spiral arteries, or to extrapolate imaging data to the functionality of the placenta.

In view of the difficulties in directly measuring placental function, there is a need to establish tools to investigate how observed pathologies in villous tree structure influence the functionality of the human placenta. Computational models are emerging as a useful tool to address this problem. Early models of oxygen delivery and uptake within the placenta placed particular emphasis on modelling the exchange of oxygen and carbon dioxide between the maternal and fetal bloodstreams at terminal villi [9, 10]. These models include detail on gas uptake dynamics but neglect the spatial flow characteristics of the maternal circulation and its resultant impact on gaseous exchange.

Later models considered maternal flow in the IVS as a porous medium [11, 12]. Erian [11] modelled the intervillous space in 2D, and assuming that the villous tree is significantly deformed by maternal flow, a flow-dependent

tissue permeability was included into their model. Chernyavsky et al. [13] combined a 3D axisymmetric porous medium approach and first order solute uptake kinetics by a homogenised villous tree (uniform porosity throughout). These porous medium models have predicted 'short-circuiting' of maternal blood flow from maternal spiral arteries to decidual veins when there are highly permeable regions in the vicinity of these arteries and veins [11], and when arteries and veins are in close vicinity [13]. In this case, there is an effective shunt as oxygenated blood does not circulate around the villous tree before leaving the IVS. This type of model also suggested that greater distances between spiral arteries and decidual veins facilitate nutrient delivery in the IVS. Chernavsky et al. [14] employed a simple model of flow and diffusion around distributed point sinks and statistical analysis of 2D placental sections to estimate the potential error incurred in homogenisation of IVS tissue to uniform or slowly varying area fractions. They showed that the accuracy of homogenisation approaches depended on flow characteristics (Peclet and Damkohler numbers), as well as the relative size of intervillous distances and typical pathlengths from spiral arteries to decidual veins. Recently, Lecarpentier et al. [15] used the Navier-Stokes equations to model blood flow between 'rigid' tissue obstacles in a 2D representation of the IVS. This approach includes significant geometric detail but is computationally expensive so does not lend itself to large scale simulations of blood flow and/or nutrient transport in the whole placenta. Serov et al. [16, 17] took a very different approach to simulating placental oxygen exchange, introducing a stream-tube model of oxygen exchange in a placental subunit. This model predicted optimal placental efficiency at tissue volume fraction that

corresponds well to those found in normal placentas. Comprehensive reviews of placental exchange models can be found in earlier publications [13, 18].

Existing placental exchange models are simplified geometrically, either by assuming that the villous tissue is homogenous with uniform uptake potential everywhere apart from at a central cavity [13], or assuming that maternal blood flow streamlines follow villous branches with oxygen uptake occurring across the surface of these branches which extends uniformly along the branch length from the central cavity to the decidual vein [16]. These geometric simplifications allow analytical (rapid) solution of models to predict function, and can be parameterised by assessment of histological slides showing the size and distribution of villous trees. These models have suggested different estimates of optimal villous tissue density for placental efficiency, with estimates from the stream-tube model comparing well to stereological data [16]. However, these models do not explicitly account for the branching architecture of the villous tree, which has been suggested to improve the accuracy of model predictions [18]. A recent multiscale model of the placental vasculature [19] suggested that vascular branching may influence placental efficiency, but did not attempt to model oxygen exchange.

Current models of oxygen exchange in the placenta assume a uniform oxygen exchange potential at any point within the villous tree structure; for example, there is no distinction between terminal and stem villi in terms of exchange barrier thickness. The harmonic mean barrier thickness between maternal and fetal blood varies through the placenta with the thinnest barriers (and most mature terminal villi) residing peripherally in the placental subunit [20, 21]. It has been theorised that peripheral villi are more ef-

fective gas exchangers than central ones, as they reside in a lower oxygen environment than central villi. A central to peripheral gradient in oxygen concentration has been confirmed in primate placental subunits [22, 23], and is consistent with hypothesised blood flow distributions [24], and has been visualised in humans using BOLD MRI [8]. To date computational models of placental oxygen exchange have not been able to account for these structural and functional inhomogeneities.

Here, we present a computational framework to model oxygen transport in a placental subunit, which aims to bridge the gap between detailed geometric models [19, 15] and highly smoothed homogeneous models [14, 13, 16, 17], providing a picture of how the architecture of the placental villi influences oxygen delivery. Like Erian's model, this modelling framework is presented in 2D for simplicity but is extendible to 3D. The model is parameterised here using morphological data and can be incorporated with imaging data. Our model predicts how maternal blood flow in a human placental subunit is influenced by a non-uniform porosity distribution over the villous structure, and whether regional variations in oxygen uptake capacity influence placental efficiency. Our aim is to examine the influences of villous tree geometry on maternal blood flow patterns, distribution of oxygen in the IVS and fetal oxygen uptake rate.

2. Materials and Methods

Our model incorporates key aspects of placental structure to simulate the distribution and uptake of oxygen within a functional unit surrounding a representative villous tree (a placentome, Figure 1b). A schematic of model

components and key outputs is given in Figure 2, and each component is described below. The model is solved using a custom written Matlab®(The Mathworks Inc., version 2012b) finite element code.

2.1. Model Geometry

Following previous studies [11], we assumed a 2D rectangular domain to represent a placental subunit (Figure 1b), which assumes that the placenta is of uniform thickness in the region of a villous tree. The domain has thickness τ, which spans the distance between the basal plate and the chorionic plate (Figure 1a), and width ω. Due to the lack of quantitative assessment of the distribution of maternal vasculature with respect to the villous trees, we followed previous studies [11, 13, 16, 17] and assumed that the placental subunit is fed by one central spiral artery (SA) and drained by two decidual veins (DVs), with one DV at a fixed distance (x_v) on each side of the SA. The SA and DVs were assumed to have a fixed diameter d.

2.1.1. Representation of the villous tree

The branching component of the villous tree has been described in several studies [6, 25, 26]. Referring to Figure 1a, the villous branches at the interface between the chorionic plate and the villous trees are termed stem villi and have a diameter of up to 1.7 mm [25]. They divide up to 15 branching generations to numerous intermediate villi (diameter around 60 μm [25]) to supply the terminal villi. The terminal villi are convoluted structures in which fetal capillaries come in close proximity to maternal blood [6]. The villus structures to the level of the intermediate villi can be considered as distinct branches for modelling purposes, but beyond that level the villus

structures become too numerous to be included individually in a model, with a branching structure that is not well described [19].

Branching component: A rule-based algorithm, described in detail in the Supplementary Material (Section A) was used to generate a villous tree structure to the level of the intermediate villi. The algorithm is controlled by the following parameters: the number of branching generations (n_b), stem length (l_s), stem diameter (d_s), daughter to parent branch length ratio (l_d/l_p), daughter to parent branch diameter ratio (d_d/d_p) and branch angle between the daughter branch and its parent branch (θ_b). These parameters, together with the condition that there must be sufficient space for a branch to grow within the domain boundary, define a bifurcating tree as shown in Figure 2, step 2. Physiological ranges for these parameters at term are given in Table 1. The most distal villi shown represent the intermediate villi. Using the parameters defined in Table 1, a villous tree comprised of 15 branching generations with 202 terminals was generated.

Beyond the intermediate villi: The convoluted terminal villi beyond the intermediate villi were modelled as homogenised 'terminal tissue blocks' (TBs), with villous tissue density as measured in stereological studies investigating the morphological properties of terminal villous tissue [2, 4]. To do this, a sampling grid was superimposed over the tree structure (Figure 2, step 3), and each element of the sampling grid containing intermediate villi was assigned to be a TB with a villous tissue area fraction (ϕ_{TV}), and an average villus diameter (d_{TV}) as given in Table 1 (Figure 2, step 4). The size of elements in the sampling grid (and so the size of each TB) was estimated to be representative of the space occupied by terminal villous tissue arising

from each intermediate villus. The cumulative length of a terminal convolute branching from an intermediate villus has been estimated to be l_{TV}=3 mm, and there are approximately n_{TV}=8-10 terminal convolutes branching from a mature intermediate villus [25]. Therefore, the area occupied by terminal villi arising from a single intermediate villus can be estimated by $l_{TV}n_{TV}d_{TV}$. The appropriate sampling grid size is then

$$\frac{l_{TV}n_{TV}d_{TV}}{\phi_{TV}}. \tag{1}$$

Based on the parameter ranges in Table 1, an appropriate sampling grid size at term is 2 mm×2 mm.

2.2. Maternal blood flow

Governing equations: To explicitly model the fluid dynamics of blood in the IVS between the numerous generations of villi would be computationally impractical even in a placental subunit. Therefore, we assume that the IVS can be represented as a porous medium [11, 12, 13]. However, we defined hydraulic conductivity ($\kappa = \kappa(x, y)$) as a spatially varying quantity calculated from the generated tree and tissue structure (Figure 2, step 5). Maternal blood flow was therefore modelled using Darcy's law:

$$\nabla \cdot \mathbf{U} = 0, \tag{2a}$$

$$\mathbf{U} = -\frac{\kappa}{\mu}\nabla P, \tag{2b}$$

where $\mathbf{U}$ is the average blood velocity in the IVS, μ is the viscosity of maternal blood, and ∇P is the local maternal blood pressure gradient.

189 *Finite element mesh and solution procedure:* The sampling grid was re-
190 fined once to obtain a finite element mesh with element size of 1 mm×1
191 mm (the maternal flow mesh). The mesh was then triangulated to obtain a
192 mixed finite element mesh and the lowest Raviart-Thomas mixed finite ele-
193 ment method was implemented to solve Equation 2 for the maternal blood
194 velocity field [27].

195 *Boundary conditions:* Pressure boundary conditions were prescribed at
196 the inlet SA ($P = P_{in}$) and outlet DVs ($P = P_{out}$). P_{in} and P_{out} were
197 fitted in the baseline case to obtain a flow velocity at the inlet element edge
198 that matches literature estimates of volumetric flow from a single SA (Q_{in}).
199 The two pressures were then held constant between simulations. Assuming
200 a total maternal blood flow of 500-750 ml/min in a term placenta [13], and
201 assuming 100 SAs [28], a value for Q_{in} of 5 ml/min is calculated. The basal
202 and chorionic plates act as barriers to flow in the IVS, so the y-component of
203 velocity was set to zero at these boundaries ($U_y(x, 0) = U_y(x, \tau) = 0$ except
204 at the inlet and outlets). At $x = 0$ and $x = \omega$, the boundaries between
205 placental subunits, a symmetry condition was applied ($U(0, y) = U(\omega, y)$).

206 *Derivation of a hydraulic conductivity field:* The hydraulic conductivity
207 coefficient in Equation 2b, was expressed using the Kozeny-Carman formula:

$$\kappa = \frac{d_{villi}^2}{180} \frac{(1-\phi)^3}{\phi^2}, \tag{3}$$

208 where d_{villi} is the average diameter of villi in the IVS and ϕ is the tissue den-
209 sity of villous tissue. Each element in the sampling grid was assigned a unique
210 isotropic κ value, which represented the conductivity of tissue branches in
211 that element or TB. The contribution to κ of the TBs is defined by ϕ_{TV}

and d_{TV}. The contribution of discrete villous branches in each element was defined using a weighted average of the diameter of villi in the element and the area occupied by branches. The maximum value of κ in each element was prescribed a value of κ_{empty}. A smooth spatially varying field for κ (Figure 2, step 5) was obtained for each element of the maternal flow mesh by sampling κ at each element of the sampling grid (Figure 2, step 3) and averaging κ over all elements surrounding each node of the sampling grid. Smoothing was then implemented via a linear interpolation to determine κ at the midpoint of each maternal flow mesh element based on the generated nodal data, and the resultant value for κ was assigned to that element.

2.3. Oxygen transport and uptake

Governing equations: Oxygen concentration in the maternal blood within the IVS (C_m) was described by the advection-diffusion equation:

$$\frac{\partial C_m}{\partial t} + \mathbf{U} \cdot \nabla C_m = D\nabla^2 C_m - \alpha(C_m - C_f), \tag{4}$$

where t is time, $\mathbf{U}$ is the velocity field calculated from Equation 2, D is the diffusivity of oxygen in maternal blood, C_f is the oxygen concentration in the fetal bloodstream and α is the oxygen uptake constant. Oxygen was assumed to be removed immediately by the fetal bloodstream upon uptake, so C_f is constant.

Finite element mesh and solution procedure: A finite element mesh comprised of bilinear elements was used to solve Equation 4 (the oxygen transport mesh). The spatial resolution of this mesh is the same as the maternal flow mesh. Equation 4 was solved using the Lagrange-Galerkin finite element

method (Supplementary Material, Section B) [29]. This is a split operator approach in which, over each time step, the departure point of blood at each mesh node is calculated and C_m at that mesh node is initiated with the concentration at the blood's departure point at the start of the timestep. The updated oxygen concentration field is then used as an initial condition to calculate the new oxygen distribution resulting from diffusion using the finite element method. Typical timestep sizes to achieve temporal convergence were $5\times10^{-6} - 5\times10^{-3}$ s. The model was solved to the steady state.

Oxygen uptake by terminal villi: At the terminal villus level, oxygen uptake was assumed to occur over the whole region bound by the TB. Using the endpoint location of each intermediate villus feeding a TB, α is distributed to each of the nodes of the sampling grid element using a bilinear interpolation function. The resulting α distribution is sampled over the oxygen transport mesh when the model was solved.

Oxygen uptake by stem and intermediate villus branches: As the stem and intermediate villus branches were explicitly modelled, α was assigned at the start and end of every branch. For each villus, α was distributed between the nodes of the oxygen transport mesh element containing the villus. The α distribution for TBs and non-terminal villi were summed to obtain an overall α distribution for solution of Equation 4 (Figure 2, step 7).

Boundary conditions: The oxygen concentration of the maternal blood entering the domain through the SA was assumed constant (C_{in}). At all other boundaries, a zero diffusive flux was imposed ($-D\nabla(C_m).\mathbf{n} = 0$, where $\mathbf{n}$ is the outward facing normal to the boundary). Oxygen is carried out of the DVs via the advective component of the solution.

2.4. Model outputs and parameterisation

Key model outputs are the flow and pressure distributions of maternal blood, the rate of oxygen uptake by the villous tree and the distribution of oxygen concentration in the IVS (Figure 2). The rate of oxygen uptake by the villous tree was computed as the difference between the concentration flux at the inlet SA and the outlet DVs, while the average oxygen content in the IVS was calculated by dividing the sum of oxygen content at all finite element nodes in the 2D domain by the total number of finite element nodes. As in previous studies, the model was parameterised to the term placenta. Nominal model parameters and ranges from the literature are listed in Table 1.

The thickness (τ) and width (ω) of the domain were chosen following Chernyavsky et al. [13]. However, estimates for placental dimensions vary in the literature. *Ex vivo* and *in vivo* estimates of placental volume are quite consistent at term [30, 31], although due to the loss of placental turgidity after delivery, placental thickness estimates vary between studies [31, 32]. For a given placental volume, the value of ω is then expected to vary with τ. Due to the lack of quantitative studies on DVs distribution over the basal plate, x_v was also chosen based on a previous model [13], where an optimum delivery of nutrients was predicted when DVs are located near the periphery of the placental subunit.

Estimation of the terminal villus density (ϕ_{TV}) varies between studies [2, 4]. The tissue density estimated by Egbor et al. [4] was used as the nominal value as the study also provided morphometric data for a variety of pathological conditions, for comparison to the healthy case. The diameter of

terminal villi (d_{TV}) is generally within the range of 0.03-0.06 mm [4, 25] and hence, a mid-range value of 0.05 mm was assigned as the nominal value.

Hydraulic conductivity is infinite in an empty sampling grid element, but allowing such data points results in sharp fronts during field fitting which is cumbersome to deal with computationally. To overcome this, the maximum κ calculated from the sampling grid was scaled up by 10 times and set as the nominal value for κ_{empty}.

The oxygen content in fetal bloodstream (C_f) was derived from oxygen measurements in the umbilical artery immediately after delivery [33], while the oxygen content in the SA (C_{in}) was based on measurements in the uterine artery collected from pregnant women during their cesarean section [34]. Conversion of partial pressure of oxygen to oxygen concentration is detailed in the Supplementary Material (Section C). The oxygen uptake constant (α) is predominantly defined by the diffusing capacity of the exchange barrier [35]. Although the properties of the exchange barrier vary regionally in the placenta, a constant 0.38 s^{-1} was set throughout the subunit as the nominal case and subsequently varied to examine how regional variation in α affects oxygen uptake efficiency.

3. Results

3.1. Baseline case, consistency with previous studies

The model makes several predictions on the whole placentome scale that are directly comparable to previous experimental and modelling studies. These predictions are described briefly here, and are included in more detail in the Supplementary Material for completeness.

Function of a placental subunit: Table 2 shows model predictions of blood flow and oxygen exchange metrics in the placental subunit under baseline conditions (using nominal parameter values). Under these conditions, the model shows consistency with experimental data, except in the ratio of venous return pO_2 to that in the IVS. This ratio is different from the ratio recorded by Schaaps et al. [34] for pO_2 in the uterine vein to the IVS. That study attributed higher measured pO_2 in the uterine vein to the vascular anastomoses in the myometrium and since such anastomoses were not incorporated in the current model, the ratio of pO_2 in venous return to IVS is expected to be different and should be less than 1.

Flow streamlines: In the baseline case, blood flow streamlines are consistent with previous model [13] and experimental [24] studies describing high flow and pressure near the SA inlets and a rapid dissipation of flow and pressure in regions comprising dense villous tissue, where blood percolates rather than streams. However, unlike the regular streamlines which conform to the hemispherical domain in earlier porous medium model due to the placement of DVs with respect to SA [13], the model generates irregular streamlines which have a tendency to pass through regions with higher hydraulic conductivity made up of non-terminal villous branches with sparse terminal tissue blocks (TBs) over areas with dense TBs, which is expected from a porous medium with spatially varying porosity.

Optimal villus density: Previous studies have assessed the relationship between villus density and oxygen exchange [13, 16], while neglecting the branching component of the villous tree. Our model comprises two components of villus density, terminal villus density, ϕ_{TV}, and a contribution from

the branching component of the tree. Our model peaks in oxygen uptake at $\phi_{TV} \approx 0.15$ (average density of all villi ≈ 0.24). This is consistent with previous porous medium model [13], in terms of optimal total villus density, but lower than the optimal villus density predicted by stream-tube model [16].

The effect of a central cavity: For consistency with previous models [11, 13], the model was solved using an artificially applied 'central cavity', represented by a relatively villus-free region with a hydraulic conductivity of κ_{empty}, having the same length and width of a typical cavity. Detailed results are given in Supplementary Material (Section D.3), and predictions are consistent with previous studies [13] in that oxygen uptake is higher in the presence of a central cavity as blood is able to penetrate further and deeper into the IVS.

3.2. Parameter sensitivity

Table 3 shows sensitivity of predictions of oxygen consumption to model parameters. Referring to Table 1, the parameters α, κ_{empty} and x_v could not be estimated directly from the literature. The model is relatively insensitive to changes in α and κ_{empty}. However, as expected, the model is sensitive to x_v. Our model shows a decrease in oxygen uptake if DVs are situated closer to SAs, consistent with previous porous medium models [13]. The predicted oxygen uptake rate is sensitive to the amount of oxygen brought into the placenta, via changes in Q_{in} (brought upon by altered P_{in} or SA diameter, d) or an altered C_{in}. Also, changes in C_f, which reflect changes in fetal metabolism, significantly influence predictions of oxygen consumption. Overall, geometrical parameters such as villous tissue density and the

branching structure of the villous tree, which is the new feature introduced in this model, have the largest effect on model predictions of oxygen consumption. This is consistent with the concept of placental branching structure having a major influence on function. Each major structural contributor to predicted function is addressed below.

3.3. The branching structure of non-terminal villi

The structure of the branching component of the villous tree (the stem and intermediate villi) plays an important role in predicted oxygen consumption. In the model with baseline parameterisation, the villous branches act as both a barrier to blood flow (via their contribution to IVS conductivity) and as an oxygen exchange surface. In addition, the distribution of branches within the IVS influences whether the villous tree is 'space-filling': large empty spaces might be expected to allow free movement of maternal blood but could potentially reduce the number, and affect the distribution of terminal villi, which are the major sites for oxygen exchange, due to space constraint.

Length of villous elements (l_s): Often, pathology is associated with a change in the balance of vessel branching and elongation [5]. While the villous tree 'fills' the placental volume, it may do so with fewer, longer branches (or conversely more, shorter branches). By changing l_s, trees with these branching properties were generated. The effect of l_s on placental oxygen uptake, the number of terminal elements in the branching tree, the amount of IVS filled with tissue (defined as the proportion of sampling grid elements containing branches or TBs), and velocity of blood emerging from the SA are shown in Figure 3. There is a non-linear relationship between l_s and oxygen

uptake rate. As l_s increases from 1.6 mm, the villous tree begins to fill more of the IVS, and so can take up more oxygen. However, as l_s continues to increase, there is a reduction in the number of villous branches that can fit into the domain, resulting in a reduction in the number of terminal villi and consequently oxygen uptake. Finally, the tree becomes sparse enough that an increase in blood flow into the IVS is possible (with the same driving pressure) with maternal blood travelling more deeply into the IVS and oxygen uptake begins to increase again. An illustration of how the villous tree fills the domain, and oxygen penetration for $l_s = 2$ mm and $l_s = 3$ mm are provided as Supplementary Material (Section E.1).

Branch angle (θ_b): Figure 4 shows the effects of varying θ_b, while holding all other parameters constant, on placental oxygen uptake, the number of terminal elements in the branching tree, the amount of IVS filled with tissue, and velocity of blood emerging from the SA. Oxygen uptake rate varies non-linearly with θ_b with a peak at $\theta_b = 24°$. The peaks in oxygen uptake correspond with peaks in velocity of blood flow emerging from the spiral artery. Although there are only small variations in the number of terminal branches and the space filling properties of the trees with θ_b, the different orientations of branches give rise to different conductivity fields. Villous branches and TBs spread out more around the inlet as θ_b increases, thereby allowing maternal blood to flow more freely into the IVS under the same driving pressure, resulting in an increase in inlet flow velocity. However, at some point ($\theta_b \geq 26°$) the gaps between the tree branches become so big that highly conductive paths are formed that shunt flow directly from the SA to the DVs, bypassing the depth of villous tissue. Oxygen uptake

is reduced as maternal blood tends to flow along this arteriovenous shunt without penetrating deep into the placental tissue. Orientation of the villous tree, flow streamlines and oxygen penetration for $\theta_b = 18°$, $24°$ and $26°$ are provided as Supplementary Material (Section E.2).

Number of branching generations (n_b): n_b was varied while holding all other parameters constant. With less than 11 branching generations, the tree does not cover the thickness of the term placenta, which is not physiological, and so n_b between 11 and 18 were considered. n_b has only a small effect on predicted flow velocity and oxygen delivery in the absence of concurrent changes in branch length or angle.

Random variability and asymmetry: An asymmetrical villous tree with random branching angles between $10°$ and $40°$ was generated to evaluate the influence of random variability of villous tree structure on model predictions. With introduction of asymmetry, a velocity boundary condition was applied at the spiral artery to obtain Q_{in} of 5 ml/min as pressure boundary conditions at the inlet SA and outlet DVs are non-applicable. While the predicted oxygen uptake rate is close to the baseline case (0.37 ml/min per placental subunit), the flow profile and resulting oxygen distribution (Figure 5) differ from the baseline case and follow an asymmetrical pattern in accordance with the conductivity field generated based on properties of the villous tree.

Optimality of uptake with variation in geometric parameters: A peak in oxygen exchange is seen with branch lengths near to normal values (estimated from anatomical studies). The model predicts that for the same placenta size, a larger number of short villous branches result in high density tissue and obstruct maternal flow and fewer long branches result in unim-

peded maternal blood circulation but smaller gas exchange surface. The model also predicts an optimum oxygen exchange when the branching angle is 24°, where villous branches and TBs are spread out sufficiently to channel maternal blood flow into the depth of the placental tissue for oxygen exchange without being shunted directly into the DVs. Without concurrent change in the branch length and angles, the number of branching generations has a small effect on oxygen exchange. The remaining model parameters, including the dimensions of the domain and maternal vasculature, blood flow and oxygen transport parameters, do not display peaks in predicted oxygen uptake within the physiological ranges analysed, although as shown in Table 3, some parameters show uniform increases or decreases in predicted oxygen uptake across the ranges considered.

3.4. The distribution of exchange interfaces

To better reflect the *in vivo* distribution of oxygen uptake described in the literature [6], the distribution of oxygen exchange surfaces was varied regionally. First, the oxygen exchange capacity (or the parameter α) was assumed to be the same at each placenta-IVS interface, but oxygen exchange was switched on and off regionally. Oxygen exchange was assumed to occur 1) evenly through the whole IVS (no influence of structure as in previous studies [13]), 2) only in terminal villi, or 3) only in stem and intermediate villi. Second, the parameter α was assumed to vary regionally according to the structural properties of villi and uptake was assumed to be 1) proportional to the average pO_2 in equally sized regions representing central and peripheral tissue, as well as basal, mid-placenta, and chorionic tissue as marked in Figure 1a of the Supplementary Material, 2) inversely proportional to the

458 average pO_2 in the regions, and 3) inversely proportional to the average
459 harmonic thickness of the villous membranes (τvm) estimated by Critchley
460 et al. [20] in the regions. Model predictions for oxygen uptake over the whole
461 placentome and average uptake per exchange interface are shown in Figure
462 6.

463 Compared with the baseline case when oxygen exchange occurs across
464 the whole villous tree, uptake by stem and intermediate villi alone results
465 in a 24.5% decrease in total oxygen uptake. However, when uptake was
466 assumed at terminal villi alone, only a 4.2% decrease is observed. In con-
467 junction with the finding that oxygen uptake rate per exchange surface was
468 1.78×10^{-3} ml/min when only terminal villi acted as exchange interfaces, our
469 model suggests that the terminal villi of the placenta are the main sites of
470 oxygen exchange in an efficient placenta. The model predicts an increase in
471 oxygen uptake from the baseline case only when α is proportional to regional
472 pO_2, or when uptake is 'easier' in high oxygen regions. This implies that
473 a placental lobule functions more efficiently when uptake occurs in regions
474 with high oxygen content (i.e., central regions). However, changes in uptake
475 rate are small (less than 1%).

476 *3.5. Diffusive and advective transport*

477 The spatial variation of Peclet number was estimated across the placental
478 subunit under baseline conditions using an average pore size of 80 μm [16]
479 as the characteristic length of the flow domain and local speed of maternal
480 flow at each node of the oxygen transport mesh. While oxygen transport by
481 diffusion is accounted for in all simulations through the use of the advection-
482 diffusion equation, oxygen transport was found to be dominated by advection

throughout the domain, with Peclet number less than 1 detected in the periphery of the placentome near to the chorionic plate. Oxygen exchange in this subchorial region is negligible as this region corresponds to the relatively villus-free subchorial lake and is supplied by oxygen-depleted maternal blood which has already passed through the oxygen exchange zone. Our model includes oxygen diffusion in the transport equation 4, which was neglected in previous porous medium models [13], and this analysis suggests that inclusion of oxygen diffusion is indeed important regionally.

4. Discussion

In this study we have presented a model of oxygen transport in a placental subunit, which incorporates key geometric features of villous tree architecture. While computational models of oxygen transport have typically focussed on the exchange dynamics at the level of the terminal villi [9, 10], or adopted a simplified homogeneous geometry for the IVS [13, 16], the current model attempts to capture the different structural characteristics of the villous tree from the stem villi to terminal villi level to provide a representative anatomically based description of how placental structures relate to their oxygen exchange function. Even though villous tree properties have been associated with different pregnancy outcomes [2, 3, 4, 36], it is unclear which geometrical features of the villous tree are most important for placental function. Here, our model provides an improved approach for the identification of key anatomical features that are crucial for placental exchange. Although the model is presented here in 2D, the composite approach employed is extendable to 3D, allowing a pragmatic approach which can be extended to

represent the whole placenta without excessive computation, and can be individualised to incorporate placental structures from high resolution imaging techniques [37, 36].

Consistency with previous studies: Our model predictions compare well to whole organ measures in terms of oxygen uptake rate and the average partial pressure of oxygen in the IVS. The predicted IVS blood flow pattern resulting from structural variations of the villous tree is consistent with the 'physiological concept' proposed in cine-angiography and injection studies [22], whereby it was postulated that streams or 'jets' of maternal blood enter the IVS and percolate radially through the densely packed villous tree due to dissipation of flow and pressure. The oxygen distribution generated by the model results also agrees with the decreasing central to peripheral oxygen gradient observed in primates [22, 23] and hypothesised in humans [24], and is also reflective of the oxygen distribution visualised in humans using BOLD MRI [8].

The effect of villous branches: Detailed descriptions of the branching of the villous tree between the chorionic plate and basal plate, which have been neglected in earlier placental exchange models [14, 13, 16], are incorporated in an oxygen transport model and used to reveal its significant role in placental oxygen exchange. First, the branching angle, length and diameter of the stem and intermediate villi, all influence how villous tree branches are spread out and fill the space in the placenta, thereby affecting how maternal blood flow is constrained and channelled in the IVS. With the baseline case, we demonstrated irregular flow streamlines which were shaped by the varying conductivity field as maternal blood tends to traverse regions of non-terminal

villous branches with sparser TBs over regions with dense TBs. Similarly, maternal blood tends to penetrate further into the IVS when the stem and intermediate villi are longer or more spread out, while villous branches with shorter length and smaller branch angles are more closely packed and obstruct maternal blood flow. The distribution of villous tissue around the SA inlet is especially important as it determines the tissue impedance to incoming flow, which in turn affects flow velocity and the path taken by the flow in the IVS. If the villous branches become too sparse, maternal blood flow will follow the path of least resistance and flow through the gaps between the villous branches and drain directly from the SA into the DVs, without penetrating deeper into the IVS. Such arteriovenuous shunting in the IVS is disadvantageous for oxygen exchange, which may also explain why villus-free margins between villous trees and the basal plate have never been observed or reported. Although previous models have suggested that shunts can arise when decidual veins are close to the spiral artery [13] or when highly permeable regions are created by villi distortion due to high speed flow near the inlets and outlets [11], our model introduces a third mechanism whereby shunts can arise due to the branching structure of the villous tree. Second, the structure of the stem and intermediate villi determines the number of terminal villi and ultimately the surface area for oxygen exchange. Since the model predicts that the terminal villi are the main sites of uptake, oxygen uptake efficiency generally increases with the number of terminals.

By changing terminal villus density alone, our model predicts an optimal oxygen uptake when the total villous tissue fraction is 0.24, which is slightly lower than the value predicted in the previous homogeneous porous

medium model of Chernyavsky et al. [13]. However, our model incorporates a branching component for the villous tree and predicts that the optimality of oxygen uptake rate is influenced significantly by the branching structure of the villous tree, and local changes in maternal blood flow profiles due to this structure. Our model, and previous porous medium models, predict lower optimal villus densities than stream-tube models, whose predictions of optimal villus density coincide with normal villus densities measured experimentally. In general, porous medium models appear to predict optimal villus density that corresponds to the total villus density in high-altitude pregnancies. Serov et al. [16] suggest several reasons for predictions of optimality to differ between the two classes of model, including the use of first order uptake kinetics (which assumes uptake is proportional to local solute concentration) and the lack of explicit representation of the uptake surface. As our model allows for local variation in villous structure, we are able to assess the implications of local variation in uptake surface by varying α regionally, however this is only a qualitative approximation and this cannot be accounted for with the accuracy possible in a stream-tube model that can explicitly describe the exchange barrier, which could explain the lower optimal villus density predicted by the model. Ultimately, validation of oxygen (or any nutrient) transport models in terms of predictions of optimality will rely on concurrent measurements of villous structure as suggested by Serov et al. [16], including artificial perfusion of the *ex vivo* placentas or primate studies to provide higher resolution data than is possible in *in vivo* human studies. Studies of *ex vivo* perfused placentas can provide information on gas exchange under different maternal and placental perfusion conditions and

oxygen levels, potentially providing validation data for both porous medium and stream-tube models. For example, introduction of different oxygen content in *ex vivo* perfusion can be used to assess whether first order kinetics is sufficient to describe oxygen exchange. *Ex vivo* perfusion studies combined with 3D structural imaging of the same placenta can also tell us more about how total exchange efficiency relates to villous structure.

To date, all models are parameterised using villous density data from stereological analysis of 2D placental cross-sectional slides. Depending on the technique employed there may be errors in representing 3D villous structures *in vivo* including the lack of maternal and fetal blood flow, artefacts that can be introduced during the fixation process, and extrapolation to 3D. Post-partum analysis of histological villous density may overestimate the *in vivo* density [16]. Currently, there is no established method to correct for these factors and to verify the *in vivo* villous density. Although 3D imaging is constantly evolving, and high throughput methods to measure villous structure in 3D would improve the quality and quantity of data, at this stage it remains arguable whether the placenta is performing at its optimal capability. Data describing the spatial distribution of blood flow and oxygen, such as MRI images, can potentially be used for validating model predictions in terms of flow and oxygen distributions and heterogeneity. Our model is qualitatively consistent with BOLD MRI distributions of oxygenation [8], but quantitative comparison is limited by difficulties in separating out maternal and fetal components in MRI. *In vivo* structural and functional imaging are evolving to give a more complete picture of the 3D placenta, with both MRI and 3D ultrasound potentially providing significant new insights into blood

flow rates and distributions in the placenta. Combining this type of imaging with *ex vivo* data in the same placentas (e.g. perfusion studies, histology, or high resolution structural imaging), provides longer-term prospects for validation of models of the placenta such as this one that predict spatial variation of flow and oxygenation.

The effect of exchange potential: Simulations assessing the effects of exchange potential within the villous tree were conducted. When there was no distinction between terminal and stem villi in terms of exchange barrier properties, oxygen exchange was found to occur predominantly at the terminal villi, in line with the current understanding of the role played by terminal villi in oxygen exchange [6]. When the exchange potential was varied as an inverse function of the average regional pO_2, the oxygen uptake efficiency is lower than when it was varied as a function of average regional pO_2, although predicted gains are small. This implies that oxygen is taken up more efficiently in regions with high oxygen content (i.e., central regions) and the uptake interfaces in these regions should possess small harmonic barrier thickness in order to optimise oxygen uptake. Critchley et al. [20] found that the mean harmonic barrier thickness is higher in the central regions as compared to the peripheral regions, showing more potential for exchange in the peripheral regions which is more akin to uptake as an inverse function of the average regional pO_2 which was predicted by the model to generate a lower uptake efficiency than the baseline case. These results differ in the presence of a central cavity where the model predicts oxygen exchange efficiency is highest when the exchange potential is varied as an inverse function of the average regional pO_2. Further studies are required to elucidate whether

structural changes observed in the exchange surfaces in low oxygen regions are beneficial to the placenta in terms of exchange efficiency.

Relevance to IUGR: Although several stereological studies have reported morphological abnormalities of the villous tree in pathological conditions [2, 3, 4], the structure-function relationship between the abnormalities of the placental villi and oxygen uptake efficiency remains hypothetical. As it is impossible to make direct measurement of the *in vivo* placenta, this model provides a channel to assess these proposed hypotheses. With the model sensitivity to villous tree geometry, the model results support the hypothesis that maldevelopment of placental villi will adversely affect placental oxygen exchange. Placentas affected by IUGR are generally smaller in volume [2, 4]. Stereological studies have revealed impoverished growth of the villi. While the villus diameter remains unaffected [2, 4], the shorter villus length [4] gives rise to a smaller villus volume and a smaller exchange surface area [2, 4]. The trophoblast epithelium was also found to be thicker [2]. A smaller placental volume (decreasing τ and ω), coupled with a smaller exchange surface area and thicker trophoblast epithelium (decreasing α) is predicted to lead to a decrease in oxygen uptake. Although a decrease in villus length (l_s) would result in an increase in oxygen uptake, the study by Krebs et al. [3] has suggested an increase in fetoplacental vascular impedance at the fetal capillary level as the capillary loops in the IUGR cases are sparse in number, generally elongated and less coiled than normal cases. The interplay of these factors is likely to contribute to an overall drop in the oxygen uptake rate. Assuming that oxygenated maternal blood enters into the IVS at a normal rate, the decrease in oxygen uptake rate would give rise to a higher

657 average pO_2 in the IVS than in normal pregnancies, which is consistent with
658 hyperoxia in the IVS as suggested by Kingdom et al. in IUGR placentas [5].

659 *Model limitations:* There are several studies which aim to quantify the
660 branching properties of villous structures [36, 38], and these studies are be-
661 coming increasingly quantitative allowing incorporation of branching and 3D
662 rotation angles [36]. Our branching villous model aims to match as closely as
663 possible to these existing studies, in terms of measured tree properties includ-
664 ing branch numbers and lengths. A sensitivity analysis to villous branching
665 parameters was conducted to assess how inaccuracies or gaps in the cur-
666 rent data may influence results. With advancements in imaging techniques,
667 anatomical studies using high resolution images (for example micro-CT) of
668 the maternal vasculature distribution and geometry of the villi can be incor-
669 porated in the current methodology to improve model accuracy.

670 In line with the 2D simplification of the 3D villous tree structure, we have
671 modified the Kozeny-Carman formula (which is typically applied to model 3D
672 media) to use the area fraction occupied by the villous tree instead of volume
673 fraction to determine a spatially varying conductivity field for approximating
674 IVS flow and oxygen transport in 2D like previous models [11, 15]. Extension
675 to 3D does not require modification of the governing equations, but does
676 require volume fraction to be used in the Kozeny-Carman formula and an
677 extension of villous branching algorithms to 3D [19, 39]. Although a 2D
678 model may not completely reflect the 3D villous geometry and flow dynamics
679 in the placenta, it is sufficient for preliminary identification of parameters
680 with major influence on placental function. Extensions of the model into
681 3D can be guided by the results of this study in their parameterisation. For

example, as the 2D model suggests branch angle is a key contributor to function, therefore this is 'a key parameter to determine' from emerging 3D imaging technologies.

Although our model assumed that the IVS is a porous medium and approximated blood flow in the IVS using Darcy's law as in previous models, our model moved away from a uniformly porous medium and took a step further by using a sampling grid to capture the regional variation in porosity based on the structure of the villous tree. In our model, a sampling grid window of 2 mm was used to capture regional variations in porosity while satisfying the assumption that the IVS is a porous medium. This is consistent with the findings of Chernyavsky et al. [14] who concluded that villous structure in a 2D section is considered as a homogenised or slowly varying porous medium if the sampling grid window size is bigger than 1 mm. Even though refinement of the sampling grid will affect the porosity distribution and give rise to a distribution that approaches the geometry of the villous tree, model solution may become unreliable since Darcy's law may no longer be suitable for approximating flow given that the assumption of the IVS as a porous medium loses its validity. Ideally, the villous tree should be represented with all its stem and intermediate villus branches as well as its terminal convolutes and maternal flow and oxygen transport should be simulated based on such detailed structures. However, given the complexities involved in representing the convoluted structure of terminal villi, we took a simplified approach of homogenising the 'random' structure of terminal villi into a tissue block with an isotropic conductivity. Also, with the lack of structural definition of the TBs, it is difficult to estimate how oxygen diffusivity varies with pore size

between villous branches. Given that our results suggest that diffusion is a minor driver for oxygen transport which only occurs mostly in the peripheral and subchorial regions of the placentome where oxygen uptake is negligible, it is reasonable to implement a uniform oxygen diffusivity of oxygen. While it is possible to account for conductivity anisotropy and regional variation in oxygen diffusivity based on the tree geometry or even solve for Navier-Stokes flow around the villous tree as demonstrated by Lecarpentier et al. [15], computational cost is an issue with such a complicated geometry, especially if flow is to be modelled on a whole organ level. For similar reasons, transport in the fetal circulation was ignored and simplified as a perfect oxygen sink, where oxygen transferred from the maternal blood was assumed to be carried away immediately by the fetal circulation. While this situation does not describe the physiology perfectly, it does help tease the effects of materno-placental blood out from those of feto-placental blood flow to help elucidate the contributions that the perfusion of maternal blood makes to placental function.

Like earlier model of Chernyavsky et al. [13], we also simplified oxygen uptake with a first order uptake kinetic by assuming that the oxygen-hemoglobin dissociation curve is linear within the pO_2 range considered in the model. In future work, the uptake kinetics could be updated to reflect the non-linear oxygen-hemoglobin dissociation behavior for a more accurate representation of oxygen exchange.

The parameter α is a measure of the diffusing capacity of the placenta, with the resistance across the trophoblast epithelium accounting for majority of the total diffusing capacity [35]. The resistance of trophoblast epithelium

varies spatially even within the terminal villi region due to the presence of locally distended fetal capillaries which give rise to vasculosyncyntial membrane with particularly thin exchange barrier. As this distribution of vasculosyncyntial membrane was only approximated by estimating the mean harmonic barrier thickness in the different regions of the IVS, in the future the model could be adapted to incorporate specific locations of vasculosyncyntial membrane to assess their influence on uptake efficiency.

5. Conclusions

We presented a placental oxygen exchange model which incorporates key geometric features of the placental villous tree. Unlike earlier models, the model captures multiple spatial scales of villous tree structure and identifies the crucial role played by villous tree geometry in efficient oxygen exchange. This modelling framework can be used and expanded upon to bridge gaps in current knowledge arising from difficulties in extrapolating animal models to the human placenta and the impossibility of performing invasive experiments on human placentas. Ultimately, with high-resolution imaging of the placenta, we expect the modelling framework to be able to predict structure function relationships in individual placenta samples while retaining computational tractability, allowing further insights into placental physiology and pathophysiology through pregnancy.

6. Acknowledgements

ML is supported by a University of Auckland Doctoral Scholarship. BM was supported by the CNRS PEPS InPhyniti funding program for his travel

to Auckland for this collaboration. This research was partially funded by a Royal Society of New Zealand Marsden FastStart grant (13-UOA-032) and a Rutherford Discovery Fellowship (14-UOA-019).

[1] T. Regnault, H. Galan, T. Parker, R. Anthony, Placental development in normal and compromised pregnancies - a review, Placenta 23 (2002) S119–S129.

[2] T. Mayhew, C. Ohadike, P. Baker, I. Crocker, C. Mitchell, S. Ong, Stereological investigation of placental morphology in pregnancies complicated by pre-eclampsia with and without intrauterine growth restriction, Placenta 24 (2) (2003) 219–226.

[3] C. Krebs, L. Macara, R. Leiser, A. Bowman, I. Greer, J. Kingdom, Intrauterine growth restriction with absent end-diastolic flow velocity in the umbilical artery is associated with maldevelopment of the placental terminal villous tree, American Journal of Obstetrics and Gynecology 175 (6) (1996) 1534–1542.

[4] M. Egbor, T. Ansari, N. Morris, C. Green, P. Sibbons, Maternal medicine: morphometric placental villous and vascular abnormalities in early-and late-onset pre-eclampsia with and without fetal growth restriction, BJOG: An International Journal of Obstetrics & Gynaecology 113 (5) (2006) 580–589.

[5] J. Kingdom, P. Kaufmann, Oxygen and placental villous development: Origins of fetal hypoxia, Placenta 18 (8) (1997) 613–621.

[6] K. Benirschke, P. Kaufmann, R. Baergen, Pathology of the Human Placenta, Springer, 2006.

[7] D. Pretorius, T. Nelson, R. Baergen, E. Pai, C. Cantrell, Imaging of placental vasculature using three-dimensional ultrasound and color power Doppler: a preliminary study, Ultrasound in Obstetrics & Gynecology 12 (1) (1998) 45–49.

[8] A. Sørensen, D. Peters, C. Simonsen, M. Pedersen, B. Stausbøl-Grøn, O. Christiansen, G. Lingman, N. Uldbjerg, Changes in human fetal oxygenation during maternal hyperoxia as estimated by BOLD MRI, Prenatal Diagnosis 33 (2) (2013) 141–145.

[9] E. Hill, G. Power, L. Longo, A mathematical model of placental O_2 transfer with consideration of hemoglobin reaction rates, American Journal of Physiology–Legacy Content 222 (3) (1972) 721–729.

[10] E. Hill, G. Power, L. Longo, A mathematical model of carbon dioxide transfer in the placenta and its interaction with oxygen, American Journal of Physiology–Legacy Content 224 (2) (1973) 283–299.

[11] F. Erian, S. Corrsin, S. Davis, Maternal, placental blood flow: a model with velocity-dependent permeability, Journal of Biomechanics 10 (11) (1977) 807–814.

[12] H. Schmid-Schobein, Conceptional proposition for a specific microcirculatory problem: maternal blood flow in hemochorial multivillous placentae as percolation of a “porous medium”, Trophoblast Research 3 (1988) 17–38.

[13] I. Chernyavsky, O. Jensen, L. Leach, A mathematical model of intervillous blood flow in the human placentone, Placenta 31 (1) (2010) 44–52.

[14] I. Chernyavsky, L. Leach, I. Dryden, O. Jensen, Transport in the placenta: homogenizing haemodynamics in a disordered medium, Philosophical Transactions of the Royal Society of London A: Mathematical, Physical and Engineering Sciences 369 (1954) (2011) 4162–4182.

[15] E. Lecarpentier, M. Bhatt, G. Bertin, B. Deloison, L. Salomon, P. Deloron, T. Fournier, A. Barakat, V. Tsatsaris, Computational fluid dynamic simulations of maternal circulation: Wall shear stress in the human placenta and its biological implications, PloS one 11 (1) (2016) e0147262.

[16] A. Serov, C. Salafia, P. Brownbill, D. Grebenkov, M. Filoche, Optimal villi density for maximal oxygen uptake in the human placenta, Journal of Theoretical Biology 364 (2015) 383–396.

[17] A. Serov, C. Salafia, M. Filoche, D. Grebenkov, Analytical theory of oxygen transport in the human placenta, Journal of Theoretical Biology 368 (2015) 133–144.

[18] A. Serov, C. Salafia, D. Grebenkov, M. Filoche, The role of morphology in mathematical models of placental gas exchange, Journal of Applied Physiology (2015) jap–00543.

[19] A. Clark, M. Lin, M. Tawhai, R. Saghian, J. James, Multiscale modelling of the feto–placental vasculature, Interface focus 5 (2) (2015) 20140078.

[20] G. Critchley, G. Burton, Intralobular variations in barrier thickness in the mature human placenta, Placenta 8 (1987) 185–194.

[21] J. Hempstock, Y. Bao, M. Bar-Issac, N. Segaren, A. Watson, D. Charnock-Jones, E. Jauniaux, G. Burton, Intralobular differences in antioxidant enzyme expression and activity reflect the pattern of maternal arterial bloodflow within the human placenta, Placenta 24 (5) (2003) 517–523.

[22] E. Ramsey, G. Corner Jr, M. Donner, Serial and cineradioangiographic visualization of maternal circulation in the primate (hemochorial) placenta, American Journal of Obstetrics and Gynecology 86 (1963) 213.

[23] R. Richart, G. Doyle, G. Ramsay, Visualization of the entire maternal placental circulation in the rhesus monkey, American Journal of Obstetrics and Gynecology 90 (1964) 334.

[24] J. Wigglesworth, Vascular anatomy of the human placenta and its significance for placental pathology, BJOG: An International Journal of Obstetrics & Gynaecology 76 (11) (1969) 979–989.

[25] R. Leiser, G. Kosanke, P. Kaufmann, Human placental vascularization, Soma H (ed): Placenta: Basic Research for Clinical Application. Int. Conf. on Placenta, Tokyo, 1990. (1991) 32–45.

[26] M. Castellucci, M. Schepe, I. Scheffen, A. Celona, P. Kaufmann, The development of the human placental villous tree, Anatomy and Embryology 181 (2) (1990) 117–128.

[27] C. Bahriawati, C. Carstensen, Three Matlab implementations of the lowest-order Raviart-Thomas MFEM with a posteriori error control, Computational Methods in Applied Mathematics 5 (4) (2005) 333–361.

[28] F. Lyall, Priming and remodelling of human placental bed spiral arteries during pregnancy - a review, Placenta 26, Supplement A, Trophoblast Research, Vol. 19 (2005) S31–S36.

[29] A. Croucher, M. O'Sullivan, Numerical methods for contaminant transport in rivers and estuaries, Computers & Fluids 27 (8) (1998) 861–878.

[30] C. de Paula, R. Ruano, J. Campos, M. Zugaib, Placental volumes measured by 3-dimensional ultrasonography in normal pregnancies from 12 to 40 weeks gestation, Journal of Ultrasound in Medicine 27 (11) (2008) 1583–1590.

[31] P. Boyd, W. Hamilton, The Human Placenta, Heffer and Sons, Cambridge, UK, 1970.

[32] J. Johannigmann, V. Zahn, V. Thieme, Utraschalluntersuchung mit dem Vidoson. elecktomedica, Elecktomedica 2 (1972) 1–11.

[33] G. Acharya, V. Sitras, Oxygen uptake of the human fetus at term, Acta Obstetricia et Gynecologica Scandinavica 88 (1) (2009) 104–109.

[34] J. Schaaps, V. Tsatsaris, F. Goffin, J. Brichant, K. Delbecque, M. Tebache, L. Collignon, M. Retz, J. Foidart, Shunting the intervillous space: new concepts in human uteroplacental vascularization, American Journal of Obstetrics and Gynecology 192 (1) (2005) 323–332.

[35] T. Mayhew, C. Joy, J. Haas, Structure-function correlation in the human placenta: the morphometric diffusing capacity for oxygen at full term, Journal of Anatomy 139 (Pt 4) (1984) 691.

[36] E. Haeussner, A. Buehlmeyer, C. Schmitz, F. von Koch, H.-G. Frank, Novel 3D microscopic analysis of human placental villous trees reveals unexpected significance of branching angles, Scientific Reports 4.

[37] S. Collins, G. Stevenson, J. Noble, L. Impey, Developmental changes in spiral artery blood flow in the human placenta observed with colour Doppler ultrasonography, Placenta 33 (10) (2012) 782–787.

[38] G. Kosanke, M. Castellucci, P. Kaufmann, V. Mironov, Branching patterns of human placental villous trees: perspectives of topological analysis, Placenta 14 (1993) 591–604.

[39] M. Tawhai, A. Pullan, P. Hunter, Generation of an anatomically based three-dimensional model of the conducting airways, Annals of Biomedical Engineering 28 (7) (2000) 793–802.

[40] J. Harris, E. Ramsey, The morphology of human uteroplacental vasculature, Contributions to Embryology 38 (1966) 43–58.

[41] G. Burton, A. Woods, E. Jauniaux, J. Kingdom, Rheological and physiological consequences of conversion of the maternal spiral arteries for uteroplacental blood flow during human pregnancy, Placenta 30 (6) (2009) 473–482.

[42] T. Goldstick, V. Ciuryla, L. Zuckerman, Diffusion of oxygen in plasma

888 and blood, in: Oxygen Transport to Tissue - II, Springer, 1976, pp.
889 183–190.

890 [43] D. Bonds, L. Crosby, T. Cheek, M. Hägerdal, B. Gutsche, S. Gabbe,
891 Estimation of human fetal-placental unit metabolic rate by application
892 of the Bohr principle, Journal of Developmental Physiology 8 (1) (1986)
893 49–54.

894 [44] E. Quilligan, A. Vasicka, R. Aznar, P. Lipsitz, T. Moore, B. Bloor,
895 Partial pressure of oxygen in the intervillous space and the umbilical
896 vessels, American Journal of Obstetrics and Gynecology 79 (1960) 1048–
897 1052.

7. Figure legends

Figure 1: (a) A schematic diagram of the human placenta at term. The placenta contains numerous chorionic villous trees which stem from the chorionic plate of the placenta into the intervillous space (IVS). Maternal blood enters the IVS from the uterine spiral arteries (SA), percolates through the IVS around the villi before draining through the decidual veins (DV). The fetal circulation resides within the villous trees, and generally runs along the branches in stem and intermediate villi before reaching a dilated and convoluted capillary structure in the terminal villi. Oxygen, nutrients and wastes are exchanged between the maternal circulation and the fetal circulation across the syncytiotrophoblast layer. (b) Model representation of a placental subunit represented by a 2D domain of thickness τ and width ω. Each subunit contains a representative villous tree generated from realistic morphometric parameters fed by a central SA and drained by two DVs. The most distal branches of the villous tree shown are termed intermediate villi, and these villi are assumed to supply 'terminal tissue blocks'.

Figure 2: Schematic showing how model components fit together for generation of model solution.

Figure 3: The effect of the length of the stem branch (l_s) on model predictions, as all other parameters were held constant. Increasing l_s effectively increases the length of all branches in the villous tree. A range of $l_s > 1.6$ was considered, as below this range the generated tree does not fill the thickness of the term placenta. (a) Oxygen uptake rate is a non-linear function of l_s.

(b) An increase in l_s gives rise to reduced number of terminal villi as the tree has fewer generations. (c) The amount of sampling grid elements containing villous tissue increases with l_s at first and then begins to slowly decrease as the tree becomes more sparse. (d) Blood flow velocity into the intervillous space is non-linear with l_s with similar changes to oxygen uptake rate.

Figure 4: The effect of branching angle (θ_b) on model predictions. (a) Oxygen uptake rate is a non-linear function of θ_b with a peak at $\theta_b = 24°$. Compared with other geometric parameters, varying θ_b results in smaller variation in (b) the number of terminal branches, and (c) the space filling properties of the generated tree. (d) Peaks in oxygen uptake correspond with peaks in blood flow velocity.

Figure 5: Flow streamlines (black lines) and normalised oxygen concentration field (colours) predicted for a placentome containing a villous tree with random branching angles correspond with the asymmetrical branching of the villous tree.

Figure 6: Oxygen uptake with different distributions of exchange interfaces compared to the baseline case where uniform uptake occurs across the whole villous tree. Oxygen exchange at non-terminal villi only resulted in a larger decrease from the baseline case than when uptake occurs at the terminal villi only. Oxygen uptake per interface is highest when exchange occurs at the terminal villi only, suggesting that the terminal villi are the main sites for efficient oxygen exchange. A small increase in oxygen uptake

948 from the baseline case is predicted when α is proportional to pO_2.

8. Tables

Table 1: Model parameters, including chosen nominal value and literature range at term.

Parameter	Description	Nominal value	Range	References
	Model Geometry			
τ	Domain thickness (mm)	20	20-45	[6, 13, 31, 32]
ω	Domain width (mm)	40	10-40	[6, 13]
x_v	Distance between SA and DV (mm)	18	unknown	-
d	Diameter of SA and DVs (mm)	2	2-3	[24, 40]
n_b	Number of branching generations	15	up to 15	[25]
l_s	Stem length (mm)	2	2	[25]
d_s	Stem diameter (mm)	1.7	1.7	[25]
l_d/l_p	Daughter/parent branch length ratio	0.975	1	[25]
d_d/d_p	Daughter/parent branch diameter ratio	0.8	$\sim$0.8	[25]
θ_b	Branch angle	18°	40°-70° (terminal branches)	[36]
ϕ_{TV}	Terminal villus area fraction	0.4	0.28-0.4	[2, 4]
d_{TV}	Terminal villus diameter (mm)	0.05	0.03-0.06	[4, 25]

Parameter	Description	Nominal value	Range	References
		Blood flow model		
μ	Blood viscosity (Pa.s)	4×10^{-3}	4×10^{-3}	[13]
P_{in}	Inlet blood pressure (mmHg)	18.8	9-12	[13, 41]
P_{out}	Outlet blood pressure (mmHg)	1.10×10^{-3}	3-5	[13, 41]
κ_{empty}	Maximum hydraulic conductivity (mm^2)	0.52	∞	-
		Oxygen transport model		
D	Diffusivity of oxygen in blood (cm^2/s)	1.62×10^{-5}	1.62×10^{-5}	[42]
C_f	Oxygen concentration in fetal blood(ml/ml)	8.72×10^{-2}	8.72×10^{-2}-2.08×10^{-1}	[33]
α	Oxygen uptake constant (s^{-1})	0.38	unknown	-
C_{in}	Oxygen concentration entering through SA (ml/ml)	1.64×10^{-1}	1.63×10^{-1}-1.66×10^{-1}	Supplementary Material (Section C), [34]

Table 2: Comparison of predicted blood flow and oxygen exchange metrics in a placental subunit simulated under baseline conditions with literature data.

Metric	Predicted value	Literature range	References
Oxygen uptake in subunit (ml/min)	0.36	0.18-0.63	[43]
Average pO_2 in IVS (mmHg)	33	23.3-33.9	[34, 44]
Ratio of pO_2 in venous return to IVS	0.90	1.48	[34]

Table 3: Percentage change in oxygen uptake rate from the baseline case with variation of the model parameters.

		% change in oxygen uptake rate	
Parameter	**% change in parameter**	**Decrease**	**Increase**
Model Geometry			
τ	10	-58.1	6.59
ω	25	20.5	119
x_v	25	-24.6	-
d	25	-38	45.8
l_s	10	41.2	-53.1
d_s	10	-54.1	-1.83
l_d/l_p	10	-	80.0
d_d/d_p	10	-55.4	-55.5
θ_b	10	-8.65	-8.16
ϕ_{TV}	10	15.0	-11.4
d_{TV}	10	21.3	-16.6
Blood flow model			
μ	10	9.75	-8.18
P_{in}	10	-9.01	8.79
P_{out}	10	1.76×10^{-4}	-1.66×10^{-4}
κ_{empty}	10	-0.16	0.012
Oxygen transport model			
D	10	2.94×10^{-4}	-2.93×10^{-4}
C_f	10	11.4	-11.4
α	10	-1.20	0.99
C_{in}	10	-21.4	21.4

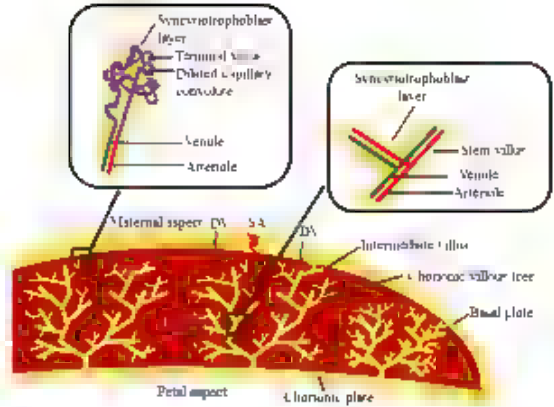
Syncytiotrophoblast layer
Terminal villus
Dilated capillary convolute
Venule
Arteriole
Syncytiotrophoblast layer
Stem villus
Venule
Arteriole
Maternal aspect
DV
SA
DV
Intermediate villus
Chorionic villous tree
Basal plate
Fetal aspect
Chorionic plate

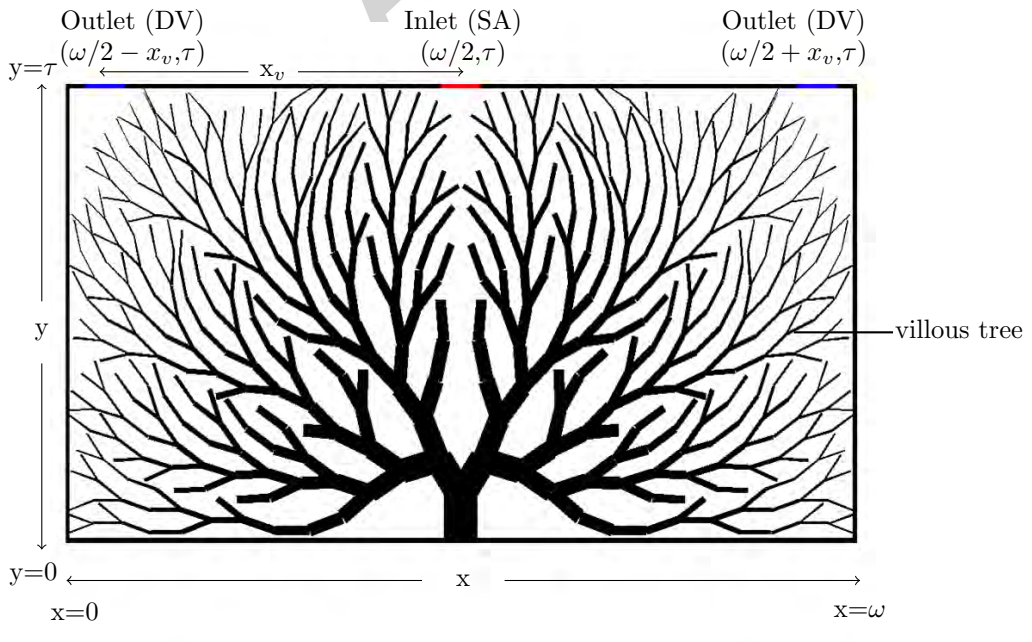
Outlet (DV)
$(\omega/2 - x_v, \tau)$
Inlet (SA)
$(\omega/2, \tau)$
Outlet (DV)
$(\omega/2 + x_v, \tau)$
y=τ
x_v
y
villous tree
y=0
x
x=0
x=ω

1. Set up domain

2. Generate tree structure

3. Define sampling grid

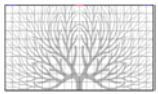

4. Fill sampling grid elements with terminal tissue blocks

5. Fit κ field using sampling grid elements as data points

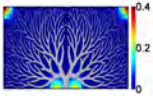

6. Predict maternal blood velocity field

a. Pressure distribution
b. Flow streamlines

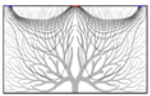

7. Distribute O_2 uptake by tissue blocks or villous branches over oxygen transport mesh nodes

8. Predict O_2 distribution in IVS

a. O_2 uptake
b. Average IVS pO_2

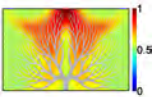

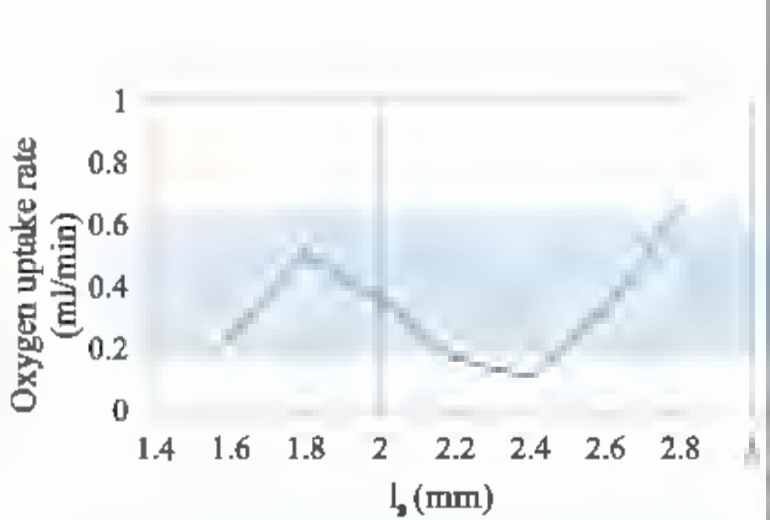
Oxygen uptake rate (ml/min)
1
0.8
0.6
0.4
0.2
0
1.4
1.6
1.8
2
2.2
2.4
2.6
2.8
l, (mm)

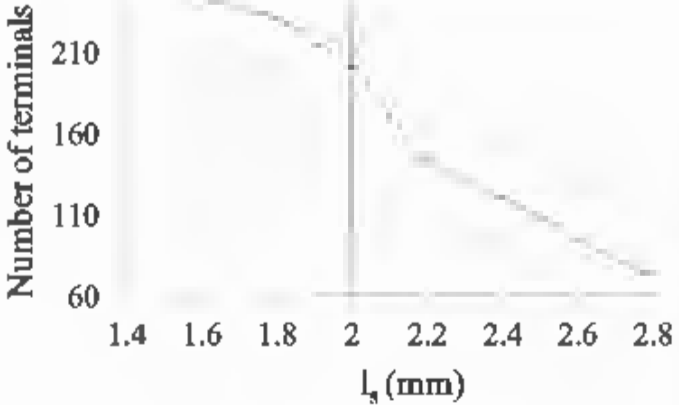
Number of terminals
210
160
110
60
1.4
1.6
1.8
2
2.2
2.4
2.6
2.8
l_s (mm)

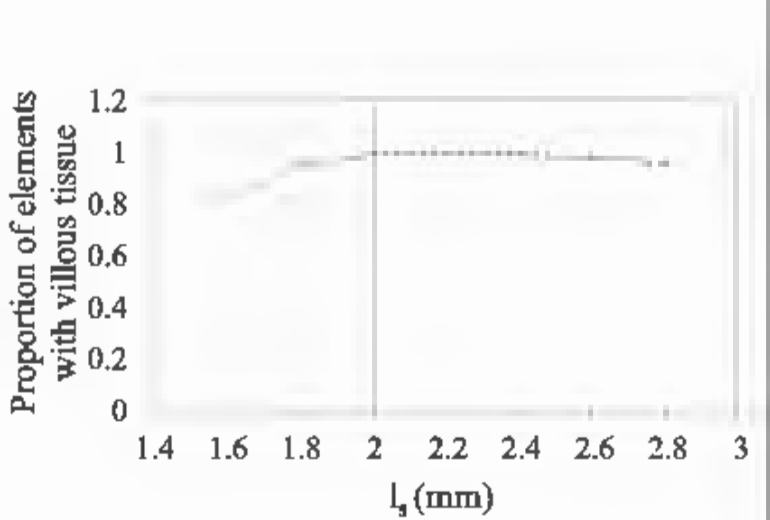
Proportion of elements with villous tissue
1.2
1
0.8
0.6
0.4
0.2
0
1.4
1.6
1.8
2
2.2
2.4
2.6
2.8
3
l_s (mm)

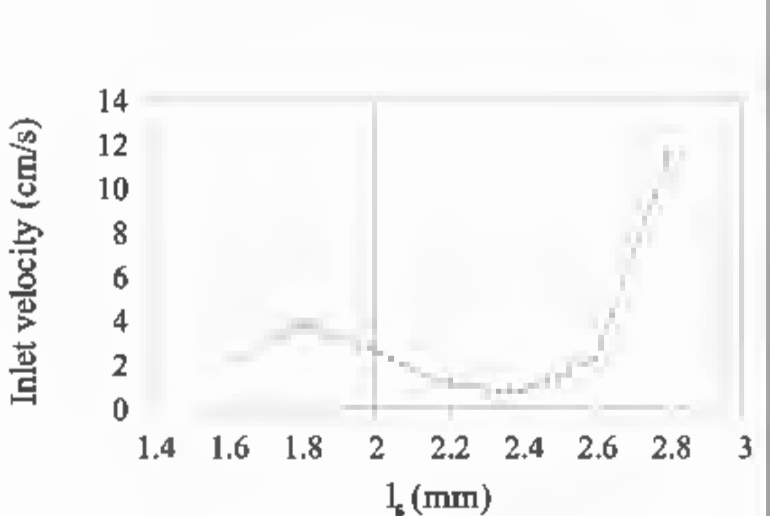
Inlet velocity (cm/s)
14
12
10
8
6
4
2
0
1.4
1.6
1.8
2
2.2
2.4
2.6
2.8
3
l_s (mm)

Oxygen uptake rate (ml/min)
1
0.8
0.6
0.4
0.2
0
5
15
25
θ_b (°)

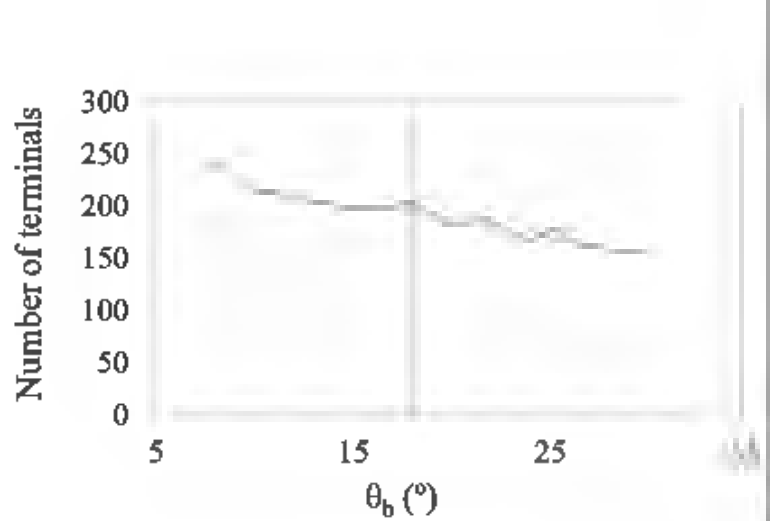
300
250
200
150
100
50
0
Number of terminals
5
15
25
θb (°)

Proportion of elements with villous tissue
1.05
1
0.95
0.9
0.85
0.8
0.75
5
15
25
θ_b (°)


Inlet velocity (cm/s)
14
12
10
8
6
4
2
0
5
15
25
θ_b (°)

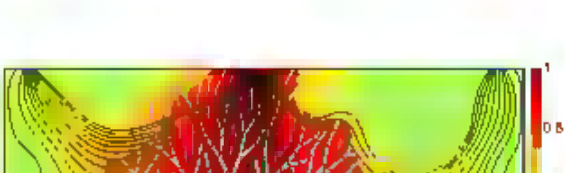
1
0.8
0.6
0.4
0.2
0

% change in oxygen uptake (overall)
5
0
-5
-10
-15
-20
-25
200
180
140
120
100
80
60
40
20
0
Even distribution
Non-terminal villi only
Terminal villi only
f(1/pO2)
f(1/vvm)
f(pO2)

Villous trees with different geometries were constructed

Villous trees were represented as non-uniform porosity distributions in model

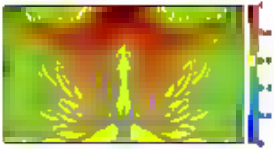

Intervillous flow pattern, oxygen distribution and uptake from different tree geometries were compared.

Oxygen exchange sensitive to villous tree structure